Engineering Failure Analysis 18 (2011) 97–109

Contents lists available at ScienceDirect

Engineering Failure Analysis

journal homepage: www.elsevier.com/locate/engfailanal

Failure analysis of a composite main rotor helicopter hub

F. Viganò [a], A. Manes [a,*], M. Giglio [a], U. Mariani [b]

[a] Politecnico di Milano, Department of Mechanical Engineering, Via la Masa 1, Milano 20156, Italy
[b] AgustaWestland, Via Giovanni Agusta 520, Cascina Costa di Samarate, VA, Italy

ARTICLE INFO

Article history:
Received 19 April 2010
Accepted 15 August 2010
Available online 26 August 2010

Keywords:
Composite rotor hub
Fatigue
Experimental
Numerical model

ABSTRACT

A full scale fatigue test of a helicopter main rotor hub MR/H has been performed by spectrum loading. The test has been supported by a detailed finite element model of the component providing relevant information about its behaviour under loading. The MR/H has been made of Ti–6Al–4V wrapped up by a circular carbon band. Stress and strain from FE model have been validated by strain survey addressing the most critical locations. Fatigue life evaluation has been carried out by analysis in good agreement with the test results. The combined approach by test and validated numerical models has proved to be a reliable tool for fatigue substantiation of critical parts.

1. Introduction

The structural integrity of the main rotor hub (MR/H) during service is a crucial task in helicopter design and maintenance strategy. A failure of this component may lead to a catastrophic effect on the whole machine. At present, fatigue evaluation of MR/H is carried out in agreement with the civil rule CS 29.571 [1], which requires that catastrophic failure due to fatigue must be avoided taking into account also the additional impact of the environment, intrinsic or discrete flaws and accidental damages. This is obtained by a combination of safe life, fail-safe, and flaw tolerant evaluations.

Nowadays deep structural analyses are conducted on helicopter hubs, and more in general on helicopter components, in order to analyze their behaviour during the application of contingent loads and to obtain the certification of the machine. In [2,3] the authors have illustrated the application of flaw tolerance methodologies dedicated on rotorcraft components. Particular attention has been addressed to the typical problem of the fatigue load scenario in helicopter structural assessment, i.e. the high frequency load cycles induced by the aerodynamic interaction of the rotor blades. The very high number of cycles per flight coupled with the presence of defects is a real big issue in the design and maintenance of modern helicopter structures. Moreover, for what concerns the rotor components the presence of interspersed high amplitude spectra like start-stop condition can influence the integrity of the structure. Thus in the last few years a very specific design methodology and approach, called ‘‘enhanced safe life”, has been developed. Particular attention has been dedicated to the near threshold fatigue crack growth, very short crack that can nucleate naturally at notches and can propagate at lower stress intensity range than the long crack threshold and at higher growth rate [2–4]. The presence of start-stop cycles, inside the high frequency flight cycles, can in fact be very dangerous and lead to a fast nucleation that can became progressively significant during the flight. This is especially important for materials like titanium alloys, whose fatigue properties are extremely sensitive to the presence of notches, heat treatment and surface condition. Of course a low stress design and frequent inspections can reduce the risk of failure, but there are some economic limits that push toward a more refined and accurate design approach. As shown in [5], a failure that occurs within a main rotor grip device is examined. From the picture of the failure section,

* Corresponding author. Tel.: +39 02 2399 8630; fax: +39 02 2399 8282.
E-mail address: andrea.manes@polimi.it (A. Manes).

1350-6307/$ - see front matter © 2010 Elsevier Ltd. All rights reserved.
doi:10.1016/j.engfailanal.2010.08.009

Nomenclature

S_y	yield stress
S_{ut}	ultimate static stress
σ_a	alternate stress of a load cycle
σ_m	mean stress of a load cycle
R	stress ratio of a load cycle
S_a	alternate stress component of fatigue limit
$S_{a,R=-1}$	rotating bending fatigue limit
$S_{aa,R=-1}$	axial fatigue limit
N	cycle number
N_f	failure cycle number
$\sigma_I,\sigma_{II},\sigma_{III}$	principal stress components
$\sigma_{Ia},\sigma_{IIa},\sigma_{IIIa}$	alternate principal stress components
$\sigma_{Im},\sigma_{IIm},\sigma_{IIIm}$	mean principal stress components
I_1	first invariant of stress tensor
I_{1_m}	first invariant of mean stress tensor
$\sigma_{Sines,a}$	sines equivalent alternate stress

reported further on in the paper, beachmarks related to a crack propagation for more than 50% of the failed area (low stress design) are clearly visible and a non-uniform fatigue striation that indicates the presence of variable amplitude loading during the life cycles can be detected. In particular the authors found this effect in the fracture initiation area where overloads and corrosion pitting promoted the fatigue mechanism.

A complete investigation of the damage tolerance capability of a helicopter hub is described in [6]. In this paper an outlook of this work for each component of the main rotor head is carried out.

According to the increasing introduction of advanced material in aerospace industry, some new researches on helicopter components are focused to study the behaviour of the composite material; Gretchen et al. [7] analyzed the fatigue life of a composite rotor hub mainly subject to delamination issues. In his work, Gretchen used a FE model and predicted the fatigue behaviour of the composite hub with good results.

Proper material properties must be taken into account for a reliable fatigue analysis and this is particularly critical in the case of titanium parts. Titanium and its alloys, in fact, have high strength, low weight ratio and outstanding corrosion resistance that are key features in a wide and diversified range of successful applications which demand high levels of reliable performance, in particular in aerospace industry.

Titanium fatigue strength of aerospace components can be influenced by many factors [8], in particular metallurgical defects, microstructural characteristics, finished surface and occasionally flaws. The main aim of this work is the analysis of a fatigue failure of a medium-weight MR/H, five-blades helicopter. This is carried out by a combined numerical and experimental approach supporting both safe life and damage tolerance evaluations.

2. Description of the component

The MR/H analyzed in this work is made of a titanium forging (Ti–6Al–4V) winded by a graphite band (see Fig. 1). Ti–6Al–4V is the most widely used titanium alloy featuring good machinability and excellent mechanical properties.

The composite band is a fail-safe device. It is a redundant solution that allows an alternative load path in the case of failure of the titanium section. The blade links are placed on the hub's handles by means of a complex elastomeric bearing. The elastomeric bearing provides flap, drag and pitch hinges with low wearing problem and high damage tolerance performance. The link with the MR/Transmission is given by a splined coupling with the MR/Mast, fitted with conical half rings, nut and bolts.

The Ti–6Al–4V hub has been obtained by a forging and machining process followed by a shot peening treatment on the whole surfaces. The composite band is obtained by a filament winding of carbon fibres inside an epoxy matrix. Artificial defects have been created in the composite filament winding in order to reproduce the worst manufacturing defects that may occur during the filament winding process.

During the flight many forces and moments act on the MR/H. In particular four kinds of forces act due to aerodynamic interaction and inertial effect of the blades in a rotating frame: centrifugal (CF), traction beam (TB), traction chord (TC) and damper (DF) forces. CF derives from inertial effects due to the rotation, TB is mainly due to the lift and TC is due to the drag of blades and an inertial component. The composition of these forces in a non-rotating frame is balanced by the hub reaction and the required forces and moments are useful to trim the helicopter. Fig. 2 shows position, direction, numbering and positive versus of each force. It is important to remark that the torque moment acting on the rotor hub, due to the section in plane force and thus the TC forces, is balanced in the real component by the rotor mast torque.

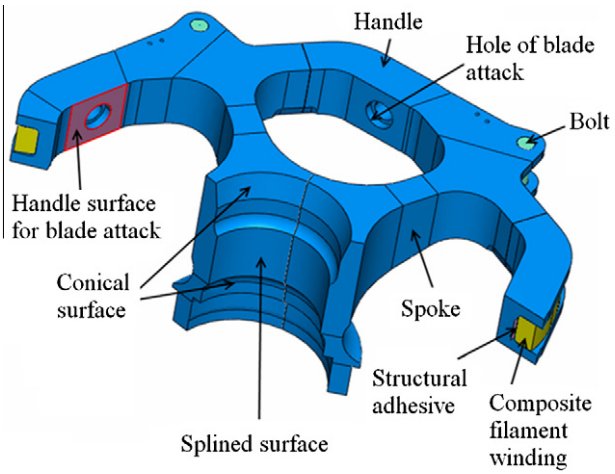

Fig. 1. Main rotor hub and its nomenclature.

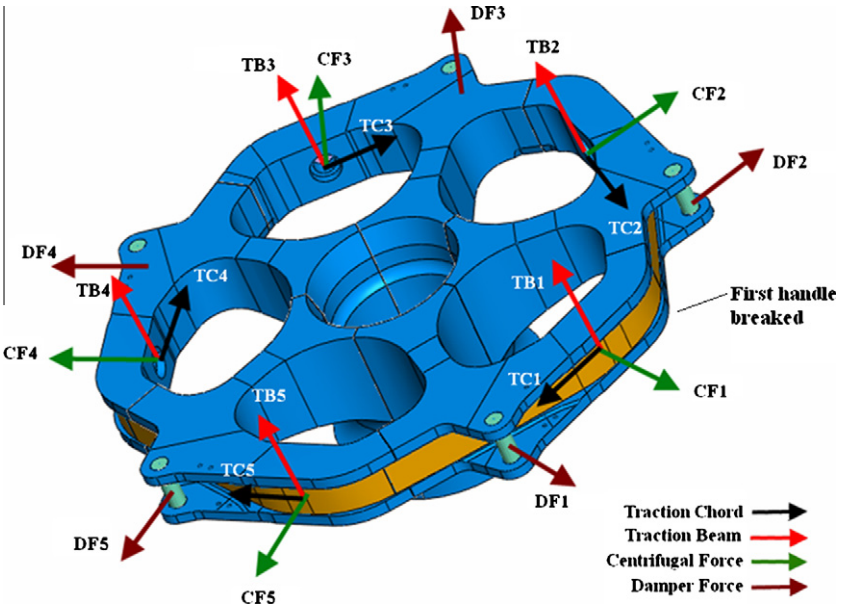

Fig. 2. Forces on the MR/H.

3. Experimental fatigue test

The aim of the test is to simulate the behaviour of the component during the application of an amplified start-stop cycle. This fatigue load spectrum simulates a significant load variation on the component which happens during the starting phase and the stop procedure of the engine-rotor system. The main aim of the test in fact has been to verify the fatigue response of the component with special attention to the blade attachments section. As we might expected this is not the only critical section in a MR/H; for example the fitting with the mast is subjected to wear during the high frequency spectrum, which simulate the steady and manoeuvred flight. A detailed description of the component is reported in the following chapter. Moreover, in order to qualify the technological process and according to the damage tolerance principles, some manufacturing discrepancies (the worst possible) have been inserted in the band technological process.

The set up of the test has been designed with the aim to apply all the main forces acting on the component in their proper magnitude and direction: traction chord (TC), traction beam (TB) and centrifugal (CF) forces. Damper forces have not been applied, having a local effect tested by another rig. Torque loading on the splined coupling is given by a TC load and the fitting to the rig has been obtained by using a simulated MR/Mast and proper fittings. Thus a complex dedicated test rig has been used for the test. See Fig. 3 for actuators and test specimen. The rig consists of a base with five 100 kN maximum force actuators for the traction chord (TC) load and a vertical structure with five 200 kN maximum force hanged actuators for the

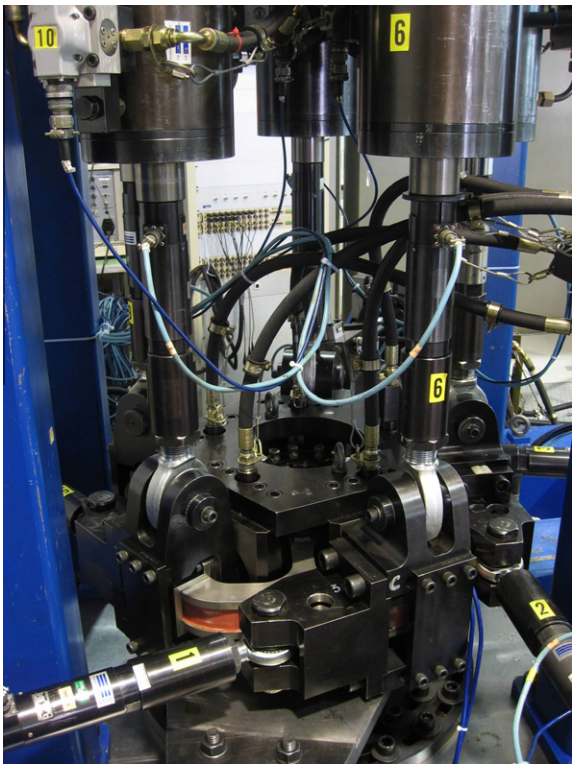

Fig. 3. The test rig with the specimen and the actuators.

traction beam (TB). Each actuator equipped with a 100 kN load cell and it applied the load in the blade attachment section. The real blade attachment with elastomeric bearing has been simulated by means of dedicated grips, properly designed for the actuators in order to have a realistic load transfer. Additional five dedicated actuators have been used inside the arms of the Hub to apply a radial load that simulates the centrifugal force (CF). The load application of these actuators has been monitored by pressure transducers. Digital command and control instrumentation have been used. The MR/Hub has been constrained to a simulated MR/Mast. Six strain gauges have been installed on the hub, also in the most critical zone. More details about their position and value are reported in paragraph 3.4 for the validation of the finite element model.

The test has been done in C4 Laboratory of Politecnico di Milano (Department of Mechanical Engineering). An amplified start-stop load spectrum, modelled by nine load steps, has been applied to the specimen, Fig. 4. The mean and the oscillatory load values have been checked to provide the required tolerance with the nominal load: 3% on the oscillatory load and 5% on the mean load.

After 31,944 cycles the test has been stopped and the component disassembled for visual inspection with NDT liquid dye penetrant test: no failure has been discovered and only minor wear has been reported in the load application zones.

After 59,032 cycles a visual inspection showed no damages. After 62,305 cycles the test has been stopped by the TC1 inferior load peak alarm. A visual inspection showed a large crack involving the whole titanium section between TC1 and TC2 actuators hinges, Fig. 5. A Non-Destructive Inspection has been carried out reporting delamination but no fibre breaking in the carbon band. The failure definitely affected the titanium section, Fig. 6.

4. The finite element model

4.1. General description of the model

A model of the whole main rotor hub subjected to the test conditions has been carried on in order to simulate the stress behaviour inside the component. In particular, the main aim of the numerical simulation has been to establish the behaviour of the different components in the damage tolerant assessment. As previously explained, the main rotor hub is in fact composed by a main classical shaped titanium hub on which a composite strap is wrapped up. Between the titanium hub and the composite winding, a film of structural adhesive has been laid.

The finite element model consists of different parts which reproduce exactly all the features of the component: geometry, materials, interactions, loads applications, constraints, etc. The finite element model has been developed using ABAQUS®v6.7 from the geometries created in CATIAV5®.

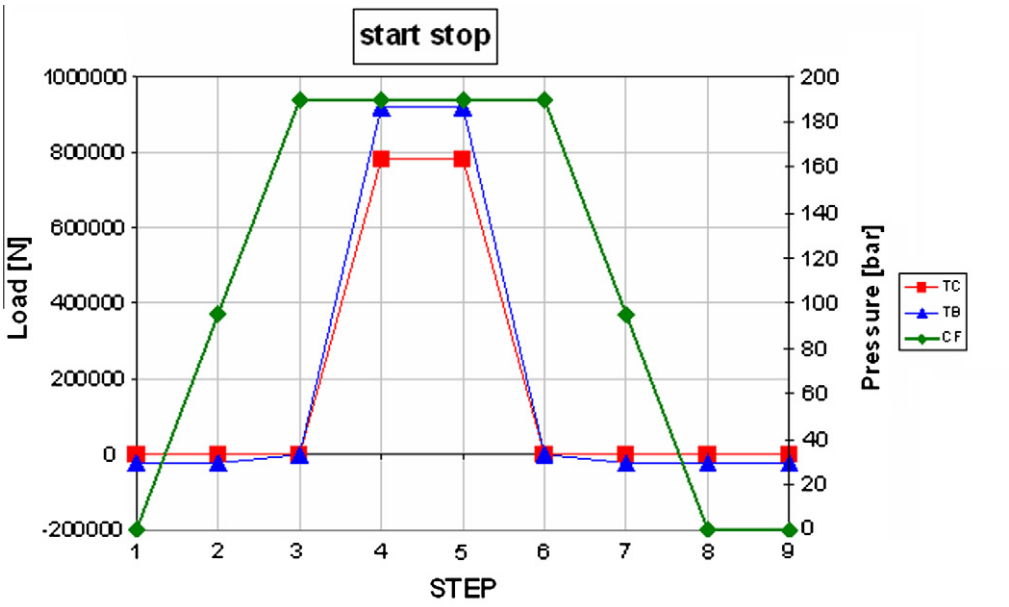

Fig. 4. The amplified start-stop load spectrum applied (CF is not in scale with TC and TB).

Fig. 5. The crack on the whole titanium section; the upper side and the lower side (in the mirror).

This geometrical model is quite complex because the need to reproduce exactly the shape of the component with the purpose to simulate the real stress distribution in detail. The geometrical model of the titanium hub has been built up taking into consideration the presence of symmetrical conditions and only one fifth of the geometrical model has been initially created, Fig. 7. Afterwards the whole model has been created with geometrical transformations, Fig. 8. Since the hub works in

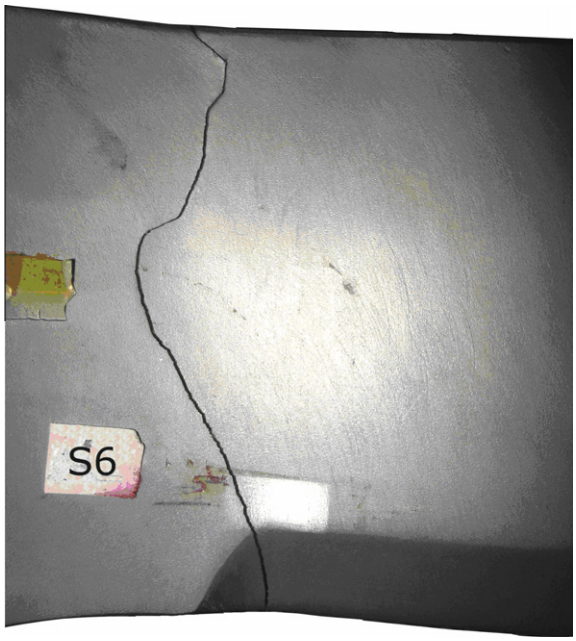

Fig. 6. The crack on the whole titanium section; a detail of the internal side: the width spot at the right of "S6" is the place of S6 strain gauge.

elastic condition during the load cycles application, titanium has been modelled as an isotropic linear elastic material with a Young modulus E = 110,300 MPa and a Poisson coefficient ν = 0.31. Three-dimensional modified quadratic tetrahedral elements (C3D10M) have been used to mesh the hub geometry (see Table 1). The zones near the notches, Fig. 7a, have a finer mesh for a correct evaluation of the stress distribution. The composite winding, Fig. 7b, has been modelled as a solid part with orthotropic, transversally isotropic material properties [9] along the winding direction. The material properties have been selected from an internal composite material database.

Between the titanium hub and the composite winding a film of AF163 structural adhesive has been positioned [10]. The adhesive film, 0.19 mm thick has been modelled as a three-dimensional solid component with continuum cohesive finite elements (COHD8) [11]. The continuum cohesive element is a specific finite element which is able to model a thin solid layer by using solid continuum formulation. The adhesive film geometry has been simplified (film rounds have been removed) in order to model it with the cohesive finite elements. This modification has been necessary because the cohesive finite element requires a geometry that can be obtained by an extrusion along the thickness (Fig. 7c). The adhesive has an isotropic linear elastic behaviour with E = 1110 MPa and ν = 0.34. As previously explained, the whole main rotor hub model, Fig. 8, has been built up fixing together all the components with complete kinematics constrains (*MPC Tie). The dumper attachment bolts, as mounted on the test specimen, have been modelled with quadratic beam elements to reproduce the correct local stiffness, Fig. 8. No manufacturing discrepancy has not been taken into consideration in the model.

4.2. Loads and constraints

As previously remarked in the experimental description the actuators transmit the loads in such a way as to reproduce the loads applied by the blades: centrifugal, chord and beam forces with hight accuracy.

Thus, loads and constraints applied to the model reproduce in full detail the real fatigue test conditions as described in Section 3 of the test set up. Three forces, applied by hydraulic actuators, act on each blade attachment. The centrifugal force (FC) of the single hydraulic actuator is applied to the surface shown in Fig. 9, the beam force (TB) and the chord force (TC) are applied to a reference point that controls cinematically the hole surface (kinematic coupling).

The constraints of the component, that reflect the real fatigue test condition, have been applied on the internal surface of the hub, Fig. 10, in suitable displacement conditions. Fitting on the MR/Mast is provided by half rings, with nuts and bolts, which block the axial motion of the MR/H thanks to the contact on the conical surface. Torque between the MR/H and the Mast is transferred by a splined coupling. In this case the torque is obviously supplied to the MR/H as a reacting action of the constraints.

4.3. FE model validation

The results of the finite element model have been compared with the strain gages measures in different load conditions to check the model validity. Fig. 10 shows the strain gauges positions. Considering a cylindrical reference system for the hub

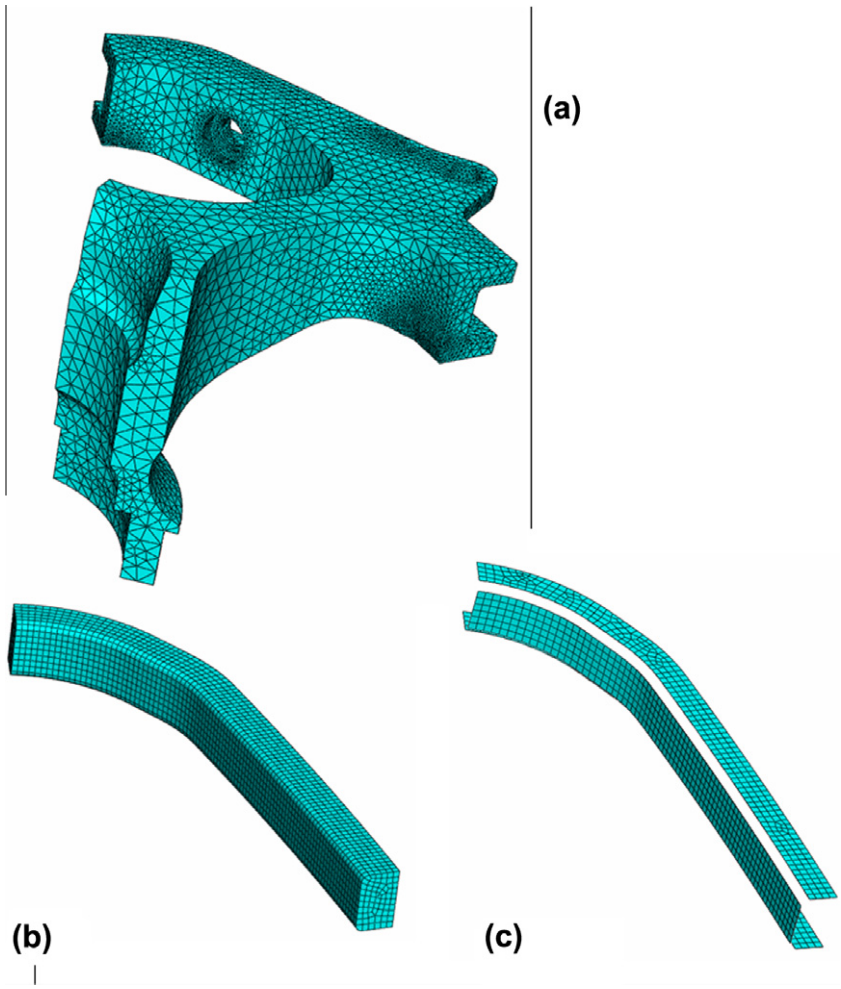

Fig. 7. One fifth geometry of the hub components meshed: (a) the titanium hub, (b) the composite winding and (c) the adhesive film.

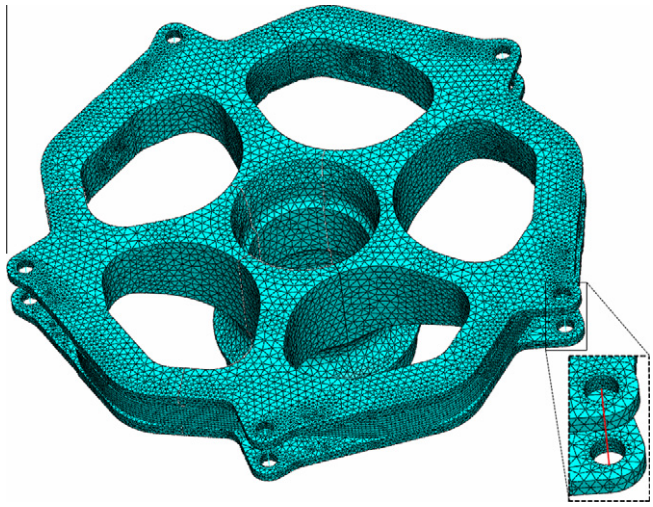

Fig. 8. The complete mesh of the main rotor hub model; the zoom shows the bolt's beam elements.

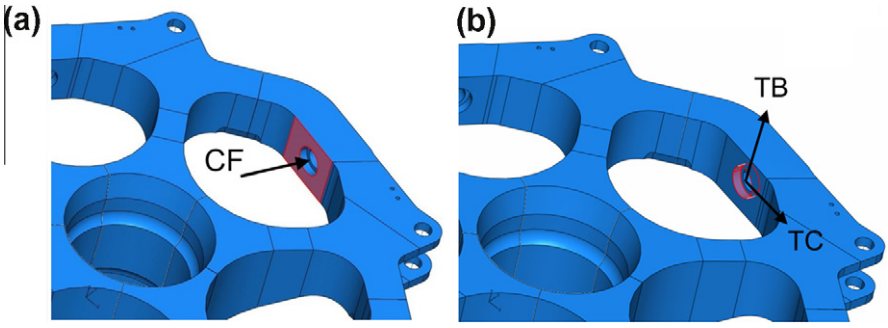

Fig. 9. The loads applied: (a) centrifugal CF, (b) chord TC and beam TB.

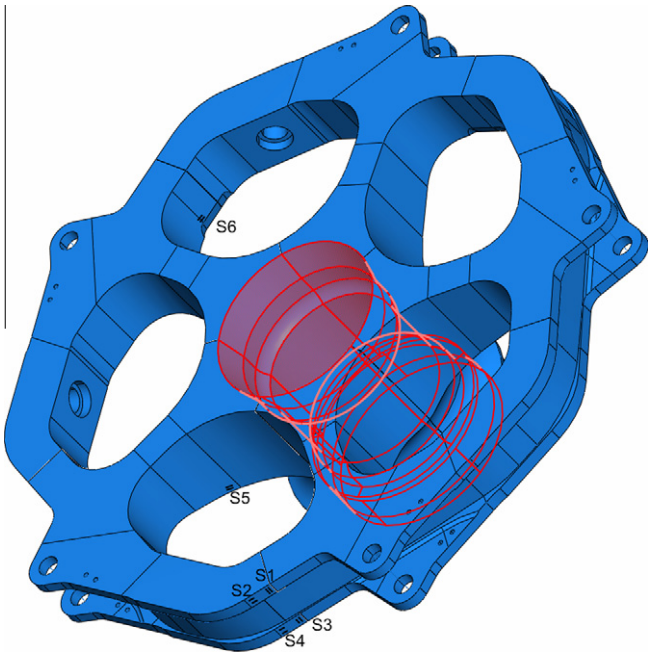

Fig. 10. The constraint and the position of the strain gauges.

Table 1
Number and type of finite element used for each component.

Component	Type of finite element	Number of elements used
Titanium hub	Three-dimensional modified quadratic tetrahedral elements (C3D10M)	278,915
Composite winding	Three dimensional quadratic hexahedral elements (C3D20)	32,775
Adhesive film	Three dimensional continuum cohesive elements (COHD8)	5520

and considering also that the axial direction is the mast axis, the strain gages S1 and S3 measure the strain in axial direction, instead S2 and S4 in tangential. The behaviour of the strain gage S6 is important for the next step, and starting from this consideration it has been fixed slightly above the notch from which the fatigue crack should start, Fig. 6. Table 2 shows the comparison between the strain gages values and the finite element results.

It is possible to state that the agreement has been very good, especially considering the complexity of the model both in terms of material properties and for its geometrical shape.

4.4. Stresses in the critical points

To carry on the fatigue life assessment it is needed to estimate the "time-history" of the stresses in the most critical zones. Considering the amplified start-stop load spectrum applied, Fig. 4, the worst load condition take place from the third to the

Table 2
Comparison between strain gages and FE results.

CF (N)	TC (N)	TB (N)	S1 (μm/m)		Error (%)	S3 (μm/m)		Error (%)
			Strain gage	FE		Strain gage	FE	
176,625	0	0	170	146	14	162	148	9
335,587	0	0	331	277	16	305	281	8
335,587	10,000	0	364	303	17	339	307	9
335,587	20,000	0	398	329	17	375	333	11
335,587	30,000	0	434	355	18	414	359	13
335,587	0	10,000	345	289	16	311	265	15
335,587	0	20,000	345	301	13	300	249	17
335,587	0	30,000	346	313	9	289	235	19
176,625	0	0	−510	−508	0	−470	−502	7
335,587	0	0	−974	−965	1	−885	−957	8
335,587	10,000	0	−1077	−1074	0	−987	−1065	8
335,587	20,000	0	−1191	−1182	1	−1109	−1173	6
335,587	30,000	0	−1308	−1290	1	−1214	−1281	6
335,587	0	10,000	−1017	−1028	1	−905	−894	1
335,587	0	20,000	−1014	−1091	8	−869	−831	4
335,587	0	30,000	−1018	−1154	13	−841	−768	9
335,587	78,000	92,000	5450	5346	2	4860	4936	2

forth step of the load cycle applied. As shown, the load ratio can be nominally considered $R = 0$. Figs. 11 and 12 show the stress when this load is applied. The critical points are positioned near the notches of the hub handle. The fatigue assessment in this critical area is carried out calculating the principal stress variation during a whole cycle. Stress direction is also relevant for a proper choice of the correct assessment criteria. Fig. 13 shows that the main stresses act in phase and the global behaviour is mainly governed by one of them. Thus, simple fatigue criteria have been chosen for the assessment.

5. Fatigue behaviour of titanium alloy

5.1. General description

The main rotor hub is made of Ti–6Al–4V (ASME F136) [12], a titanium alloy which is one of the most used materials in high performance components in aerospace, marine and chemical industry. The Ti–6Al–4V alloy is a $\alpha + \beta$ alloy, containing 6% aluminium and 4% vanadium, with high mechanical properties ($S_y = 900$ MPa, $S_{ut} = 1030$ MPa), lightness and corrosion resistance. However, the fatigue behaviour of the Ti–6Al–4V alloy is highly influenced by its microstructure and by the operations which are made during the manufacturing cycle (i.e. forging, shot peening and rolling).

The titanium microstructure depends on the thermal cycle which the material is subject to, both during heat treatments and during manufacturing process.

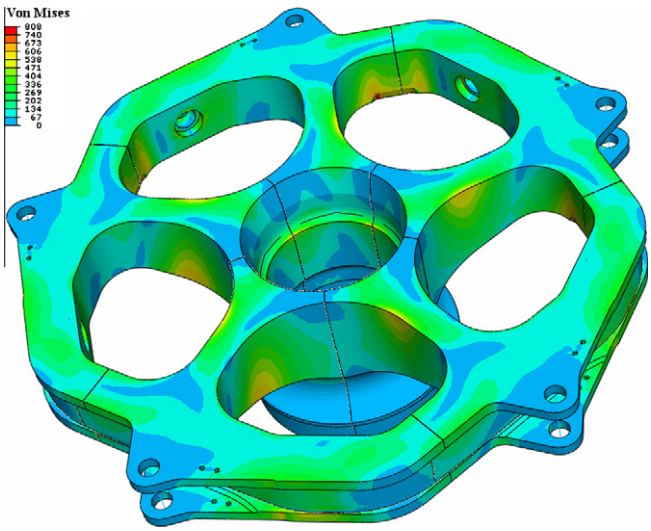

Fig. 11. FEM results in the worst load condition.

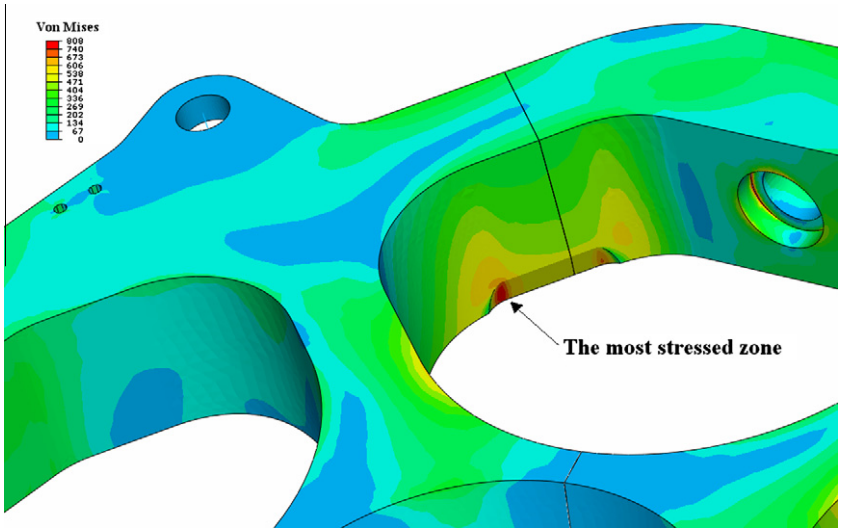

Fig. 12. Enlargement of FEM results in the hub's handle.

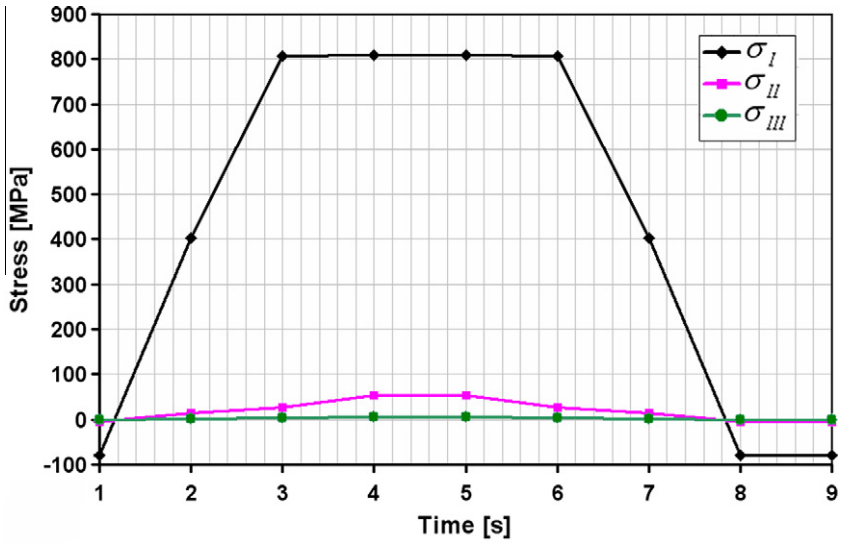

Fig. 13. Principal stresses in the most stressed area.

The thermal cycle governs the distribution of α and β phases in the titanium microstructure. In fact, Ti–6Al–4V heated above the phase transition temperature T_β (995 °C), shows only phase β which is characterized by a cubic centred crystal reticule.

Under temperature T_β, α and β phase are present together in the microstructure thanks to the presence of aluminium and vanadium; α phase is characterized by a hexagonal compact crystal reticule.

The forging temperature plays a fundamental role in high-cycle fatigue (HCF) performances; if Ti–6Al–4V is forged just below the phase transition temperature, the microstructure obtained will have a fatigue limit higher than the fatigue limit of the microstructure obtained forging above T_β (15%, more).

Another important factor is the heat treatment. There are two kinds of treatment for Ti–6Al–4V alloy: the annealing treatment and the solution treatment with age-hardened.

The annealing treatment consists of heating the material at a temperature between 700 and 850 °C – 1–4 h followed by slow cooling.

Solution treatment usually consists of heating the material at 950 °C followed by a quenching in water. Ageing treatment usually consists of heating the material at 500 °C – 3–6 h and allow the solution treated titanium to increment its static mechanical properties.

Table 3
Coefficients of Eqs. (1) and (2) for each fatigue database; all the data refer to load ratio $R = -1$.

Fatigue database	Testing condition	A	B
ESDU™	Rotating bending	−4.824	18.079
	Axial	−6.672	22.833
MIL-HDBK-5J	Axial	−3.783	14.984

The annealing confers titanium a better fatigue behaviour than solution treatment with age-hardened treatment. To give the best fatigue properties, the main rotor hub has been forged by preheating the material at a temperature just below T_β and after exposing it to annealing treatment.

Shape and dimensions of the component are factors which can modify the HCF properties. Simple shape and small dimensions help to lead to a uniformity of distortion (due to forging) along the cross section and consequently to higher fatigue limit.

Surface condition is also a factor which influences the fatigue behaviour; the titanium alloy Ti–6Al–4V is affected by surface roughness, nicks and gouges. These factors, for example, are the cause of 30% fatigue cracks in titanium hub of H-46 US Navy helicopter's [13].

The surface of the hub has been shot peened to induce residual compression stresses that reduce the surface notch sensitivity [14]. With the surface shot peened the fatigue crack nucleate internally, where the zone with compressive residual stress is mitigated; that was exactly what happened to a titanium hub of a Royal Netherlands Navy helicopter [8].

5.2. Fatigue data

The experimental data used for the fatigue life evaluation have been taken from MIL-HDBK-5J [15] and ESDU™ database [16].

The military handbook MIL-HDBK-5J describes the mechanical properties of the materials used in aerospace vehicles. In the MIL handbook the fatigue data of Ti–6Al–4V in different manufacturing forms and with different heating treatments are reported. All the fatigue tests on Ti–6Al–4V have been made using axial alternate load on specimens.

Another fatigue data source is the Engineering Science Data Unit (ESDU) database. In ESDU database are present 1200 fatigue results about Ti–6Al–4V in each supply form, dimension and heating treatment. In ESDU database, there are both axial fatigue and rotating bending fatigue data of Ti–6Al–4V forged (bellow T_β) and annealed.

To have a good approximation of the low cycles fatigue life zone of Whöler diagram, the bilogarithmic model (1) has been used for each fatigue database:

$$\log N = A \cdot \log S_a + B \tag{1}$$

where S_a is the fatigue limit of rotating bending and N is the cycle number to failure. The terms A and B of the model were calculated according to a minimum square error method.

For axial fatigue data, the model used (Eq. (2)) has been the same but the axial fatigue limit (S_{aa}) has been taken into account instead of the rotating bending fatigue limit:

$$\log N = A \cdot \log S_{aa} + B \tag{2}$$

The forged (below T_β) and annealed fatigue data which refer to Ti–6Al–4V of each fatigue database have been interpolated and the results are reported in Table 3. Together with the linear regression model the confidence interval of the cycle number to failure has also been calculated.

5.3. Influence of mean stress

The mean stress (σ_m) affects the alternate fatigue limit (S_a or S_{aa}); there are different models able to take into account this effect. The influence of σ_m on S_a depends on the cycle number to failure; at 10^5 cycles Gerber equation is probably the best model which approximates the fatigue data.

6. Fatigue assessment criteria

Both monoaxial and multiaxial fatigue assessment criteria have been used to estimate fatigue life. The state of stress in the critical point is in fact mainly monoaxial, Fig. 8, consequently simple equations can be used to estimate fatigue life with satisfactory approximation.

In this way the calculation of N_f (cycle number to failure) has been made by solving the Gerber equation both for rotating bending fatigue data Eq. (3) and for axial fatigue data Eq. (4).

Table 4
Fatigue evaluation results.

Fatigue database	Type of test	Fatigue criteria	N_f	C.I. at 95%	
				$N_{f,min}$	$N_{f,max}$
ESDU	Rotating bending	Monoaxial	106,692	91,831	123,957
		Sines	120,038	91,773	157,007
	Axial	Monoaxial	57,252	42,953	76,311
		Sines	67,498	51,616	88,267
MIL-HDBK-5J	Axial	Monoaxial	56,068	40,988	76,696
		Sines	60,384	45,870	79,492

C.I. = Confidence interval.

$$\sigma_a = S_{a,R=-1}(N_f) \cdot \left(1 - \left(\frac{\sigma_m}{S_{ut}}\right)^2\right) \tag{3}$$

$$\sigma_a = S_{aa,R=-1}(N_f) \cdot \left(1 - \left(\frac{\sigma_m}{S_{ut}}\right)^2\right) \tag{4}$$

In order to taken into account the other stress components a multiaxial criterion has been chosen. The state of stress during the start-stop load cycle application is located in the elastic field and with proportional behaviour (in phase); thus the Sines criterium can be used [17]. According to the Sines rule the failure can occur (with a probabilistic approach) when Eq. (5) is satisfied.

$$\sigma_{Sines,a} = S_{aa,R=-1}(N) - k(N) \cdot I_{1_m} \tag{5}$$

The term $\sigma_{Sines,a}$ is the Sines equivalent stress and it is defined by the following equation:

$$\sigma_{Sines,a} = \sqrt{\sigma_{Ia}^2 + \sigma_{IIa}^2 + \sigma_{IIIa}^2 - \sigma_{Ia}\sigma_{IIa} - \sigma_{Ia}\sigma_{IIIa} - \sigma_{IIa}\sigma_{IIIa}} \tag{6}$$

I_{1_m} is the first invariant of the mean stress tensor and it is defined by the following equation:

$$I_{1m} = \sigma_{Im} + \sigma_{IIm} + \sigma_{IIIm} \tag{7}$$

The term k is defined by the relationship:

$$k(N) = \left(\frac{S_{aa,R=-1}(N)}{S_{aa,R=0}(N)} - 1\right) \tag{8}$$

The term $S_{aa,R=-1}(N)$ has been taken directly from the fatigue model described in Section 4.2; the term $S_{aa,R=0}(N)$ has been estimated from $S_{aa,R=-1}(N)$ using the Gerber model to consider the mean stress.

7. Results

In Table 4 the results of N_f evaluation obtained from the combination of different fatigue data and fatigue criteria are reported.

The fatigue test results shows that fatigue crack occurred between 59,032 and 62,305 cycles. Fig. 14 shows that the results obtained using axial fatigue data predict well the resulting fatigue. Otherwise, the life calculated from rotating bending fatigue limit overestimate the experimental fatigue life probably due to an overestimation of the fatigue limit in this load condition, not so fit for the assessment with FE results. The results show also that life estimations according to the Sines rule are higher than monoaxial evaluation.

8. Conclusions

Because of the need to certify a critical helicopter component, a full scale test on a titanium-composite MR/Hub was done with the failure of the component: the details and results are reported in the present paper. After the application of an amplified start-stop load spectrum a failure has occurred in the handle of the titanium hub between 59,032 and 62,305 load cycles. During the failure of the titanium part, the composite band remained undamaged and carried out the fail-safe functionality correctly. Further tests and numerical activities (not described in this article) have been done on the damaged component to check the residual strength and thus certify the damage tolerance capability too. However for what concern the test reported, a finite element model of the MR/H has been developed and the stress distribution has been estimated correctly up to the fatigue failure. A fatigue life evaluation has been done using fatigue data obtained from two different database containing both rotating bending fatigue limit and axial fatigue limit of the material. All the fatigue data processed refer to a Ti–

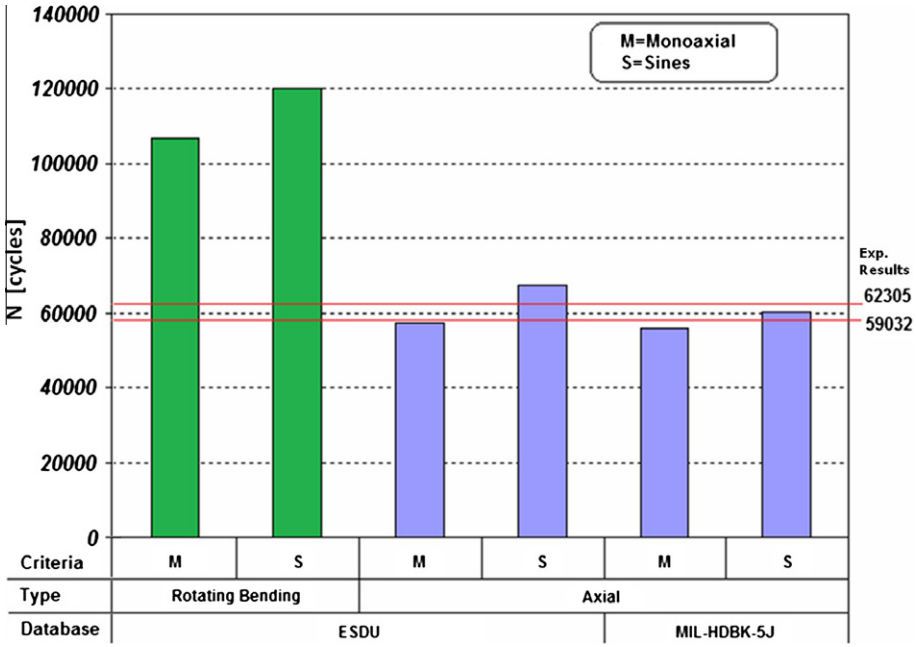

Fig. 14. Histogram of fatigue life prediction.

6Al–4V forged just below T_β and annealed. Because of the state of stress, both monoaxial and multiaxial (Sines) fatigue criteria have been followed. The fatigue life estimation based on axial fatigue limits are in good agreement with the experimental result. Moreover the FE model shows an important stress concentration exactly in the point in which the fatigue crack nucleated.

To conclude, it is possible to state that although the full scale tests remain necessary in order to asses the fatigue behaviour of complex components, numerical models can play an important role and can be used successfully also in complex life predictions like fatigue behaviour. However, the fatigue life prediction and assessment are very hard work with a lot of uncertainties [18]. Correct simulation of the specimen and accurate characterization of the material are important issues to achieve a reliable result with a numerical model. In addiction to this a correct understanding of the relevant fatigue load spectra is an important condition to carry out correctly the experimental test. A multilevel, multidisciplinary approach is therefore necessary for the design of such a complex component.

References

[1] CS-29 – Certification specification for large rotorcraft. European Aviation Safety Agency, November; 2008.
[2] Mariani U, Vicario M. Application of flaw tolerance methodologies to rotorcraft fatigue qualification. European Rotorcraft Forum 2005.
[3] Lazzeri L, Mariani U. Application of damage tolerance principles to the design of helicopters. Int J Fatigue 2009;31:1039–45.
[4] Tiong UH, Jones R. Damage tolerance analysis of a helicopter component. Int J Fatigue 2009;31:1046–53.
[5] Lourenço NJ, Von Dollinger CFA, Graça MLA, de Campos PP. Failure analysis of the main rotor grip of a civil helicopter. Eng Fail Anal 2005;12:43–7.
[6] Biasini M, Mariani U, Oggioni F. EH101 – Main rotor head components evaluation of the damage tolerance capability. Eur Rotorcraft Forum 1996.
[7] Murri GB. Testing and life prediction for composite rotor hub flex beams. Int J Fatigue 2006;28:1124–35.
[8] Wanhill RJH. Material-based failure analysis of a helicopter rotor hub. J Fail Anal Prev 2003;3:59–69.
[9] Kollar LP, Springer GS. Mechanics of composite structures. Cambridge University Press; 2003.
[10] 3M – Scotch-Weld structural adhesive film AF 163-2 technical data, November; 2004.
[11] SIMULIA - Abaqus analysis user's manual. Version 6.7; 2008.
[12] Ratner BD, Hoffman AS, Schoen FJ, Lemons JE. Biomaterials science: an introduction to materials in medicine. Academic Press; 2004.
[13] Cammett JT. Analysis of H-46 helicopter rotor head component fatigue cracking. In: Proc 42nd international SAMPE symposium; 1997. p. 904–14.
[14] Madayag AF. Metal fatigue: theory and design. John Wiley & Sons; 1969.
[15] Department of Defence – MIL HDBK-5J - Metallic materials and elements for aerospace vehicle structures, January; 2003.
[16] ESDU™. Fatigue of wrought and cast Ti–6Al–4V Titanium alloy – engineering sciences and data unit, January; 2008.
[17] Socie DF, Marquis GB. Multiaxial fatigue. SAE International; 1999.
[18] Schijve J. Fatigue damage in aircraft structures, not wanted, but tolerated? Int J Fatigue 2009;31:998–1011.